SCIENCE AND TECHNOLOGY ORGANIZATION
CENTRE FOR MARITIME RESEARCH AND EXPERIMENTATION

Reprint Series **CMRE-PR-2019-032**

Doppler passive fathometry

Chris H. Harrison

May 2019

Originally published in:

The Journal of the Acoustical Society of America, volume 144, issue 2, August 2018, pp. 577–583, doi: https://doi.org/10.1121/1.5048941

About CMRE

The Centre for Maritime Research and Experimentation (CMRE) is a world-class NATO scientific research and experimentation facility located in La Spezia, Italy.

The CMRE was established by the North Atlantic Council on 1 July 2012 as part of the NATO Science & Technology Organization. The CMRE and its predecessors have served NATO for over 50 years as the SACLANT Anti-Submarine Warfare Centre, SACLANT Undersea Research Centre, NATO Undersea Research Centre (NURC) and now as part of the Science & Technology Organization.

CMRE conducts state-of-the-art scientific research and experimentation ranging from concept development to prototype demonstration in an operational environment and has produced leaders in ocean science, modelling and simulation, acoustics and other disciplines, as well as producing critical results and understanding that have been built into the operational concepts of NATO and the nations.

CMRE conducts hands-on scientific and engineering research for the direct benefit of its NATO Customers. It operates two research vessels that enable science and technology solutions to be explored and exploited at sea. The largest of these vessels, the NRV Alliance, is a global class vessel that is acoustically extremely quiet.

CMRE is a leading example of enabling nations to work more effectively and efficiently together by prioritizing national needs, focusing on research and technology challenges, both in and out of the maritime environment, through the collective Power of its world-class scientists, engineers, and specialized laboratories in collaboration with the many partners in and out of the scientific domain.

NOTE: The CMRE Reprint series reprints papers and articles published by CMRE authors in the open literature as an effort to widely disseminate CMRE products. Users are encouraged to cite the original article where possible.

Doppler Passive Fathometry

Chris H. Harrison[a)]
Emeritus Scientist, Centre for Maritime Research and Experimentation, Viale San Bartolomeo 400, 19126 La Spezia, Italy

(Received 3 May 2018; revised 6 July 2018; accepted 18 July 2018; published online 3 August 2018)

Passive fathometry is a technique whereby broadband ambient ocean noise received on an array of hydrophones is averaged and cross-correlated to produce a sub-bottom profile [Siderius, Harrison, and Porter (2006). J. Acoust. Soc. Am. **120**, 1315–1323]. Here this technique is extended to determine the vertical velocity of the array, and compensate for it, without any prior knowledge, i.e., Doppler Passive Fathometry. For Fourier transform lengths beyond a certain limit, the differing Doppler between the direct and bottom reflected paths spoils the correlation match, however it is shown by using some experimental data, where the array was known to suffer from arbitrary but near periodic motion, that compensation is possible, enabling continuing time integration. In the process, the vertical velocity becomes known. Velocity, with peak value $\sim\pm 1$ m/s, is plotted against time and shown to be 90° out of phase with depth, as expected for periodic motion. Since stationary targets have already been detected by noise correlation [Harrison (2008). J. Acoust. Soc. Am. **123**, 1834–1837], it is implied that the range of moving targets can also be determined.
 https://doi.org/10.1121/1.5048941

[SED] Pages: 577–583

I. INTRODUCTION

Ocean ambient noise received on a vertical array of hydrophones can be beamformed vertically into upward and downward endfire beams. "Passive Fathometry" (PF) consists of cross-correlating these two beams and time-averaging to form an impulse response of the seabed and sub-bottom layers beneath the array (Siderius *et al.*, 2006). Since these layers are typically well stratified and near horizontal, horizontal array motion is not only tolerated, it adds the ability to construct sub-bottom profiles (Harrison and Siderius, 2008). In contrast, vertical motion is more problematic, and may result from unwanted wave-induced motion, or attempts to reconcile long integration times with desired platform motion (e.g., autonomous underwater vehicles, AUVs). One might imagine that the cross-correlation, being a broadband process, would be immune from Doppler effects, which are usually thought of in the frequency domain as a frequency shift. Despite the fact that the envisaged vertical velocities are very small, the Doppler effect can be understood in the time domain as a stretching or shrinking of the time sequences to be correlated. So if the array is traveling upwards, the direct path time sequence is slightly shrunk, whereas the bottom reflected path is simultaneously slightly stretched. This means that the vital, exactly vertical components (Harrison and Siderius, 2008) of the upward and downward sequences that, without motion would match perfectly, no longer match. Under certain conditions this effect can be serious, warranting specialised processing. The rest of this paper justifies this assertion and proposes a criterion for the onset of the requirement for Doppler processing that depends on array speed, number of samples in the block to be cross-correlated, and various filter settings. This type of mismatch problem could also be considered to be a special case of the generalized distortions tackled by wideband ambiguity functions often invoked in the signal processing literature (Goh and Goodman, 2013).

Other considerations to be borne in mind include the implications for PF using adaptive beam forming (Siderius *et al.*, 2010; Harrison, 2009, 2018), detection of point targets as opposed to reflecting surfaces (Harrison, 2008, 2016), and other geoacoustic inversion techniques (Muzi *et al.*, 2015; Quijano *et al.*, 2012; Yardim *et al.*, 2014).

In Sec. II the effects of stretching and shrinking is abstracted from underwater acoustics by taking a simple filtered random number sequence as the starting point. This establishes the behaviour and a criterion for the cross-correlation peak being degraded or not. In Sec. III real experimental data from BOUNDARY 2004 are analysed in the region where this criterion suggests that the peak may, or may not, be degraded depending on processing parameters. In the potentially degraded case the solution of un-shrinking the data by interpolation before processing is proposed. Inevitably there are complications such as known vs unknown motion, non-uniform motion, already determined experimental sampling rates that make re-sampling difficult, and so on. These are discussed in Secs. III and IV.

II. SIMULATION OF CROSS-CORRELATION WITH DIFFERENTIAL DOPPLER

In reality the surface noise sources have no special location or orientation relative to the hydrophone array, and the detailed emergence of the Green's function after time averaging has been described generally (Roux and Kuperman, 2004; Roux *et al.*, 2005; Sabra *et al.*, 2005) and specifically

[a)]Visiting Professor at Institute of Sound and Vibration Research, University of Southampton, Highfield, Southampton SO17 1BJ, United Kingdom. Electronic mail: chris.harrison1946@gmail.com

for a vertical array (Siderius *et al.*, 2006). However, of all these sources, only the ones exactly vertical above the source (specifically, within a Fresnel zone) are effective after time integration (Harrison and Siderius, 2008). For this reason the following simulation concentrates on the effect of stretching and shrinking this single path and ignores the many paths from other sources, which would ultimately be eliminated by integration. The sound source is taken to be a single smoothed N-point random number sequence with Gaussian probability distribution and variance of one, with a corresponding set of times each separated by δt where $\delta t = 1/f_s$ and f_s is a notional sampling rate. It is assumed that the array moves vertically at upward velocity v producing a time domain Doppler shrinking in the direct path by a factor D and a stretching in the reflected path by a factor $1/D$. The problem is to construct a stretched and a shrunk sequence from this original, but still sampling at a single rate in order to facilitate digital cross-correlation. Shrinking (i.e., bunching the waveform up) is done by defining a set of new, slightly larger, time intervals (actually $\delta t_{\text{new}} = \delta t \times D$, to which the original waveform is interpolated. These interpolated numbers are then essentially "read out" at the original sampling rate to make a shrunk sequence. Stretching is the opposite process (i.e., $\delta t_{\text{new}} = \delta t \,/\, D$). In the current context the velocities are so small compared with the speed of sound c that the distinction between a Doppler factor of $D = 1 + v/c$ and $D = 1/(1 - v/c)$ is negligible and will be ignored. Needless to say, the difference between the direct path and reflected path factors is not negligible, being $2v/c$. Essentially a filtered random number sequence r_n has a (digital) auto-correlation function $A_m = \sum_n r_n\, r_{n+m}$ but when the single sequence is both shrunk and stretched by interpolation to form, respectively, r_n^{shrink} and r_n^{stretch} this becomes a cross-correlation $C_m = \sum_n r_n^{\text{shrink}} \times r_n^{\text{stretch}}$ that depends on the amount of stretch, i.e., D or v.

Piece-wise linear interpolation is adequate as long as the original sequence has already been low-pass filtered. Thus the features of the waveform are preserved even when the exact sample points vary. This is known as "band limited interpolation" (Crochiere and Rabiner, 1983). In contrast, with experimental data, where the sample rate is predetermined, one might have to resample at a higher rate [e.g., by upsampling or using fast Fourier transform (FFT) zero-padding] before continuing with linear interpolation. To be compatible with the experiments described in Sec. III the random number sequence had a notional sampling frequency of 120 kHz (ten times the actual experimental value) with a low-pass filter at 4 kHz, close to the design frequency of the experimental array.

For a given autocorrelation time (i.e., bandwidth) and total time duration, the properties of the cross-correlation function can be investigated numerically as a function of D or array velocity v. As D increases from unity, one expects an increasing mismatch between the two sequences, leading to a broadening and reduction in height of the initial delta function correlation peak. This is plotted for several velocities against sample number in Fig. 1. Figures 2(a) and 2(b) show, respectively, the (linear) width and height variation as a function of velocity.

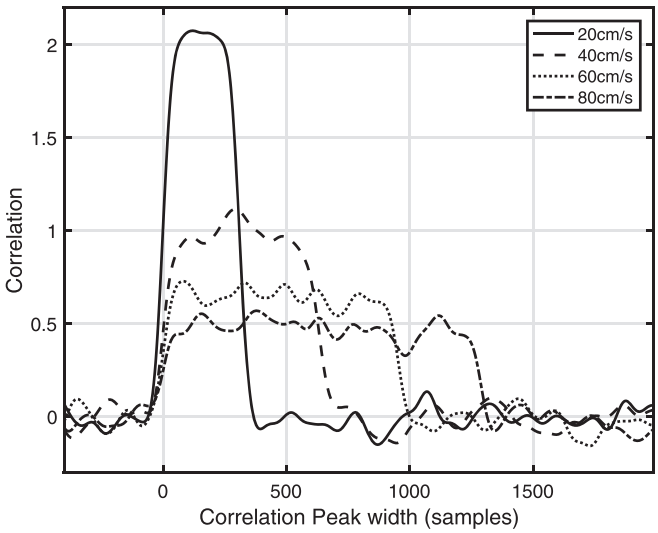

FIG. 1. Enlargements of the correlation peak for a random number sequence correlated with a Doppler-shifted, i.e., time-domain-stretched, version of itself. Curves for four vertical velocities are shown.

The integrand of the correlation, i.e., the product of the shrunk and stretched functions of time without any offset and before integration, is shown in Fig. 3(a) for $v = 0.5$ m/s; perhaps a simpler way to visualise the increasing mismatch is to plot the *difference* between them as in Fig. 3(b). Initially on the left there is no disagreement between the two functions since they are well aligned, but as time increases the discrepancies increase more or less linearly until (fairly suddenly) reaching the limit of no correlation whereupon the envelope flattens out [in Figs. 3(a) and 3(b)]. This transition point, marked with a dashed line, forms the basis for a practical criterion since it separates the region on the left, where alignment up to that time is reasonably good, from the region on the right, where, by that time, the time offset between the two waveforms is enough to degrade any correlation completely.

The practical criterion, or rule-of-thumb, for the onset of a mismatch within the given time T and therefore the requirement for special Doppler processing can be devised as follows. A Doppler mismatch would begin at time T when the stretched waveform has overtaken the shrunk waveform by one autocorrelation "cycle," a time Δt that depends on the initial low-pass filtering, i.e., the effective bandwidth. In other words

$$T^{\text{stretch}} - T^{\text{shrink}} = T \times D - T/D \approx 2\,(D-1)\,T = \Delta t. \tag{1}$$

Inserting an "engineering factor," α, of order unity to allow a number of cycles tolerance, this can be rearranged as a critical time T_c beyond which special Doppler processing will definitely be required to mitigate the correlation degradation. It is, in fact, exactly the location of the dashed line in Fig. 3, having chosen $\alpha = 1.5$,

$$\begin{aligned} T_c &= \frac{\alpha\,\Delta t}{2\,(D-1)} \\ &= \frac{\alpha\,\Delta t\, c}{2\,v}. \end{aligned} \tag{2}$$

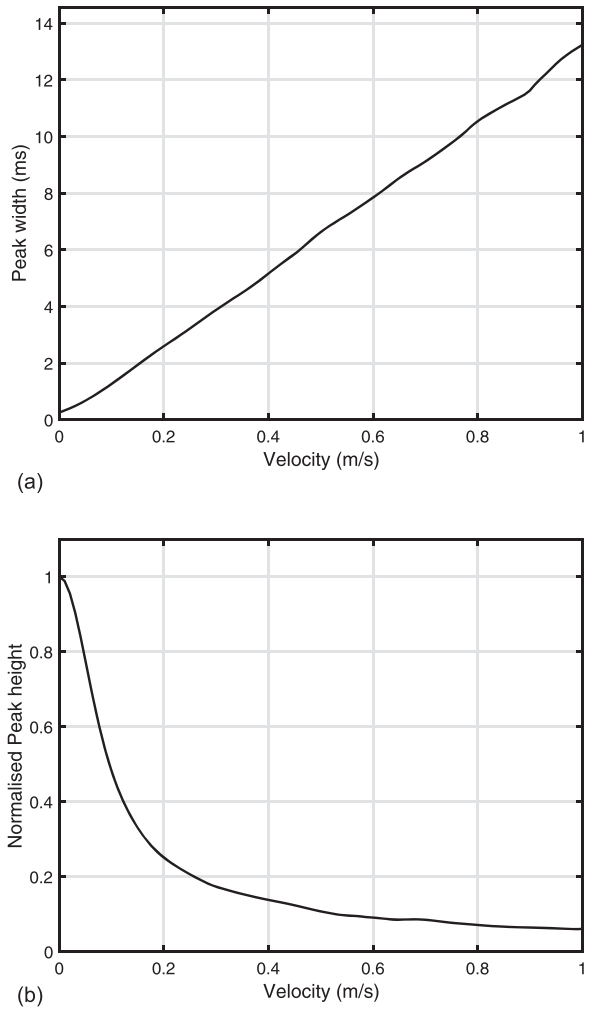

FIG. 2. (a) Correlation peak width vs velocity, i.e., time-domain stretching (10 ms corresponds to 1200 samples in Fig. 1); (b) peak height vs velocity.

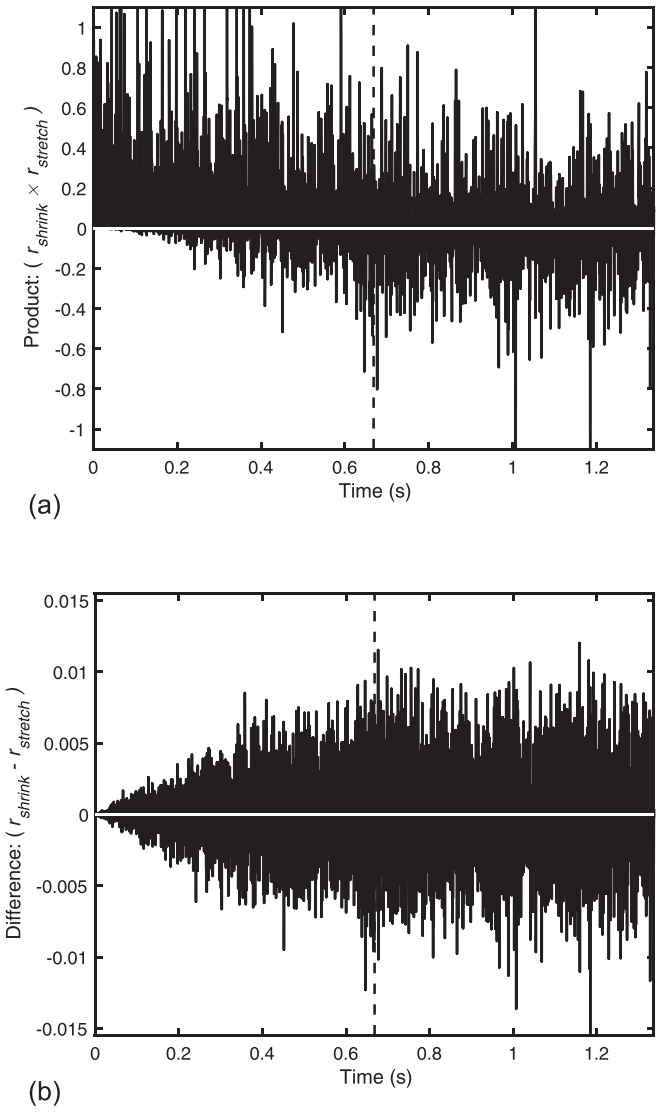

FIG. 3. Degeneration of the correlation integral shown as (a) the integrand, i.e., the product of the shrunk and stretched terms, r_n^{shrink} and r_n^{stretch}, (b) their difference. The dashed line indicates the critical time T_c.

As an example, the experimental data described in Sec. III had a bandwidth, w, of about 4 kHz, i.e., $\Delta t = 1/w = 0.25$ ms. The array motion is seen in Traer and Gerstoft (2011) and Harrison (2017) to have an amplitude of about 1 m and a period of 7 s which implies a maximum vertical velocity of just over 1 m/s. So assuming $\alpha = 1.5$, $c = 1500$ m/s, $v = 1$ m/s results in a critical time of $T_c = 0.2812$ s. Comparing this figure with the size of FFTs used by those authors, i.e., 4096 at a sample rate of 12 kHz with duration 0.34 s, shows that success was borderline and confirms the (unpublished) finding that larger FFT sizes do not work in these circumstances.

In milder sea states, such as 2003 BOUNDARY (Harrison and Siderius, 2008; Harrison, 2017, 2018) where the (unknown) array velocity might be less than, say, 10 cm/s then $T_c = 2.812$ s and FFT sizes of 16 384 (duration 1.36 s at 12 kHz sampling) are, and were, tolerated without any special processing.

III. DOPPLER PROCESSING OF EXPERIMENTAL DATA

Experiments in the Mediterranean in 2003 and 2004 with a 32-element drifting vertical array with hydrophone separation 0.18 m and therefore design frequency of 4.167 kHz have been described and analysed before (Harrison and Siderius, 2008; Harrison, 2005). The 2004 data were obtained in bad weather, and there is compelling evidence that the array was moving up and down with an amplitude of about 1 m and a period of about 7 s (Traer and Gerstoft, 2011; Harrison, 2017). These data are processed below in such a way that any array motion is allowed for. The particular recordings analysed here start at 15:44:56 UTC on May 12, 2004 which is taken as zero drift-time in all figures. Depths (distance between reflecting layer and array centre) are displayed as two-way path length in metres. In all cases there happen to be two reflections about 4 m apart centred around 110 m.

The reason for choosing this particular time during the experiment is not to do with the performance of Doppler Passive Fathometry (DPF). Rather it is simply that to demonstrate that DPF *does* work it seems wise to use as a benchmark the data where array motion has already been deduced from the two-way travel time (see Traer and Gerstoft, 2011; Harrison, 2017). However the standard PF technique is severely limited by integration time issues under these

conditions, so there are only limited times when successful PF results are available with clear array motion.

A. Processing: Detailed approach

Harrison (2017) mentions three equivalent methods of computing the noise cross-spectrum for a stationary array: (1) form the product $\mathbf{d}^\dagger\mathbf{C}\mathbf{u}$, where $\mathbf{C}$ is the CSDM and $\mathbf{u}$, $\mathbf{d}$ are up and down steering vectors; (2) form the product $\mathbf{d}^\dagger\mathbf{H}\mathbf{u}$, where $\mathbf{H}$ is the separated Hankel part of the CSDM; (3) at each temporal frequency form the product of the sum over all hydrophones weighted, respectively, by an upward and a downward steering vector [*ibid.*, Eq. (39)]. [Note that there is a typographic error in Eq. (39). When compared with Eqs. (36)–(38), the second term on the right of both lines should be conjugated.] The third approach is adopted here for a moving array since it offers clarity in allowing independent processing of the upward and downward beams. Section III C will return to the issue of other possible approaches including adaptive beamforming.

First, a plausible set of vertical velocities is postulated, and the following processing steps taken for each one. By investigating the result which is a function of travel time and chosen velocity one can pick the best velocity, and one can also continue processing despite the motion.

The steps of the processing are as follows:

(1) Take the FFT of all 32 hydrophone channels $y_{j,k}$ assuming nominal frequencies and a sample rate of 12 kHz to form the matrix $x_{j,k}$, where j is the hydrophone index and k is the frequency sample index

$$x_{j,k} = \mathrm{FFT}(y_{j,k}). \tag{3}$$

(2) Upsample x by a factor of 10 to facilitate later linear interpolation. Although this is introduced because of the well-known implications for interpolation of sampled data by arbitrary factors, in practice the resulting differences in depth profiles are negligible, but the differences in velocity are perceptible though small.

(3) Form steering vectors at each nominal (upsampled) frequency f_k, where z_j are the hydrophone depths and c is sound speed, as

$$\begin{aligned} w^U_{j,k} &= \exp\left(iz_j 2\pi f_k/c\right), \\ w^D_{j,k} &= \exp\left(-iz_j 2\pi f_k/c\right). \end{aligned} \tag{4}$$

(4) Take the sum of the products

$$\begin{aligned} p^U_k &= \sum_{j=1}^{N} x_{j,k} \times w^U_{j,k}, \\ p^D_k &= \sum_{j=1}^{N} x_{j,k} \times w^D_{j,k}. \end{aligned} \tag{5}$$

(5) Interpolate linearly from the nominal (upsampled) frequencies f_k to the Doppler up-shifted frequencies $f_k{}^U$ and the down-shifted frequencies $f_k{}^D$,

$$\begin{aligned} q^U_k &= \mathrm{interpolate}(f_k, p^U_k, f^U_k), \\ q^D_k &= \mathrm{interpolate}(f_k, p^D_k, f^D_k). \end{aligned} \tag{6}$$

(6) Get the (upsampled) cross-spectrum as

$$S_k = q^U_k \times (q^D_k)^*. \tag{7}$$

(7) Convert the cross-spectrum to an impulse response s_k, a function of time by Inverse Fourier Transform (IFFT)

$$s_k = \mathrm{IFFT}(S_k). \tag{8}$$

Note that the samples of s_k are automatically determined at the original time-sampling intervals regardless of the upsampling at step (2).

Within this third processing option from Harrison (2017) there are still alternatives, for instance, in step (4), instead of multiplying x by the weight at the nominal frequency, one could separately interpolate x to the up- and down-shifted frequency and multiply by the corresponding weight calculated at the up- and down-frequencies, then skip the interpolation of step (5).

B. Processing results

1. Improved depth profile plot

There are still two free processing parameters: Fourier transform (FT) length and number of cross-spectra [step (6)] to average. Bearing in mind that overlapping FTs are permissible and that the total time must be short enough to assume the velocity to be constant, the FT size was chosen to be 16 384 with 4 overlapping FTs uniformly spaced every 0.17 s (2048 samples) in drift-time. This contrasts with the shorter 4096-sample FT used in Harrison (2017) which was chosen to avoid the Doppler issue but still resolve the layers.

Assuming no vertical motion, analysis leads to a profile as shown in Fig. 4(a). Although there is a hint of waviness with period around 7 s, the motion is not clear. In fact the "blobs" at about 37, 40, 46, 50, 57, 61 s coincide with the array being stationary at the peaks and troughs of the array's motion, as will be seen.

The amplitude in Fig. 4(a) appears to be about 1 m, so with a period of 7 s one expects a maximum velocity of just less than 1 m/s. In the following examples 13 array velocities were postulated at equal spacings between +1 and −1 m/s, the central one being zero. In principle each velocity can provide a plot in the same format as Fig. 4(a). Plots for +0.5 m/s and −0.5 m/s are shown in Figs. 4(b) and 4(c). The upward velocity plot shows an enhancement (in strength) in the intervals from depth maximum to depth minimum but degradation from depth minimum to maximum. The opposite behaviour is seen for downward velocity.

A simple way of demonstrating the improvement over the zero velocity assumption is for each depth and drift-time (i.e., pixel) to take the maximum strength over all assumed velocities. The result is shown in Fig. 4(d) where a clearer continuous wave motion is seen. The same (logarithmic) scales are used in Figs. 4(a)–4(d).

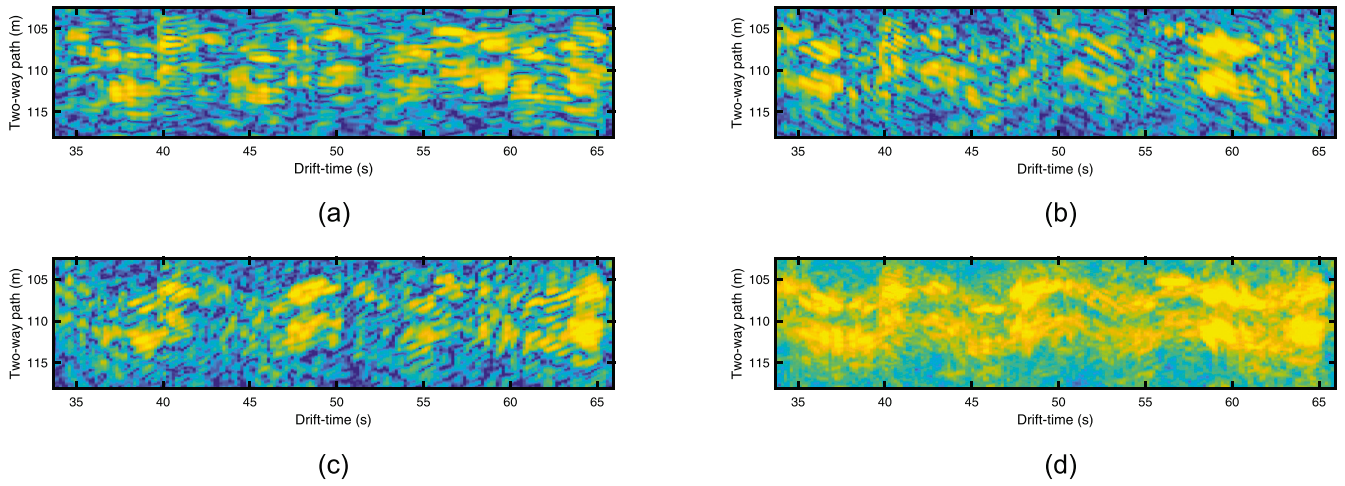

FIG. 4. (Color online) Impulse response as two-way path length vs drift-time for various assumed receiver vertical velocities: (a) 0.0 m/s, (b) +0.5 m/s, (c) −0.5 m/s, (d) the maximum intensity taken over all 13 assumed velocities. Intensity on arbitrary dB scale between −45 and −32.

2. Velocity vs drift-time

The starting point is an intensity P that is a function of two-way path length (between 102.5 and 118 m), drift-time, and velocity. To obtain velocity vs drift-time the mean of P is taken over all path lengths (between 104 and 117 m) at each drift-time, then these values are smoothed in the velocity dimension with a Gaussian weighting of width ∼0.5 m/s. The result is shown in Fig. 5. There is a clearly visible, periodic oscillation.

This can be taken one step further by finding the velocity from Fig. 5 that has the maximum intensity at each drift-time. Applying a 1 s smoothing in drift-time to these velocities results in the wavy line of velocity vs drift-time seen superimposed in Fig. 6. Increasing the number of chosen velocities from 13 to say, 21, decreases the pixelation in Fig. 5 but has little effect on the line in Fig. 6.

3. Velocity superimposed on depth vs drift-time

To make sure that these velocities agree with the already known two-way path lengths a wavy depth line can also be obtained from a threshold crossing in Fig. 4(d), applying similar filtering. Figure 7 shows the (scaled) velocities of Fig. 6 superimposed on this depth line. It can be seen that, as expected, when depth is decreasing, upward velocity is at a maximum, and when depth is increasing, upward velocity is at a negative maximum.

By cross-correlating velocity and depth (Fig. 8) one can see the 7 s periodicity with a zero of correlation very close to zero offset which indicates a phase difference of almost exactly 90° as expected.

4. A check against the critical time criterion of Eq. (2)

The discussion after Eq. (2) arrived at a critical time for this experiment of $T_c = 0.2812$ s. On the one hand this means that the FFT size of 16 384 (duration 1.36 s) used throughout this section *did* require special Doppler processing whereas an FFT size of 4096 (duration 0.34 s) was borderline, but on the other hand a 4096-FFT has little chance of separating velocities.

C. Processing postscript

In retrospect the processing used here where, for clarity, the cross-spectrum was computed directly from the product of FTs, clearly works but is not the only possible processing. The three methods from Harrison (2017) mentioned in Sec. III A above were shown to be exactly equivalent in the zero velocity case. However it can be seen that the equivalence can be extended to the case where velocity is significant. As suggested in Sec. III A, processing step (4) can be replaced by the product of a pre-interpolated x (i.e., x^U, x^D) and steering weights calculated at the up- and down-shifted frequencies

$$q_k^U = \sum_{j=1}^{N} x_{j,k}^U \times \exp\left(iz_j 2\pi f_k^U/c\right),$$
$$q_k^D = \sum_{j=1}^{N} x_{j,k}^D \times \exp\left(-iz_j 2\pi f_k^D/c\right). \quad (9)$$

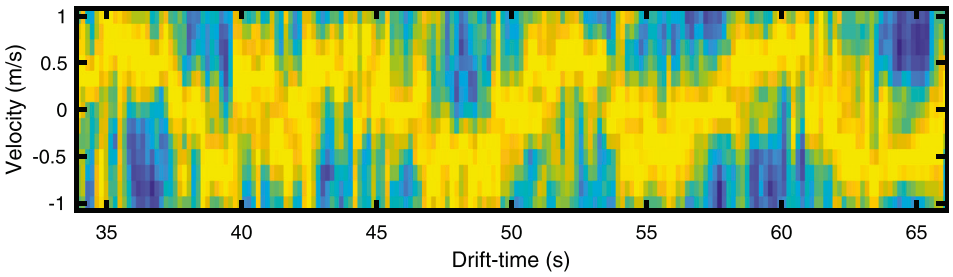

FIG. 5. (Color online) Vertical velocity derived from 13 trial values at each drift-time. Linear normalised intensity scale.

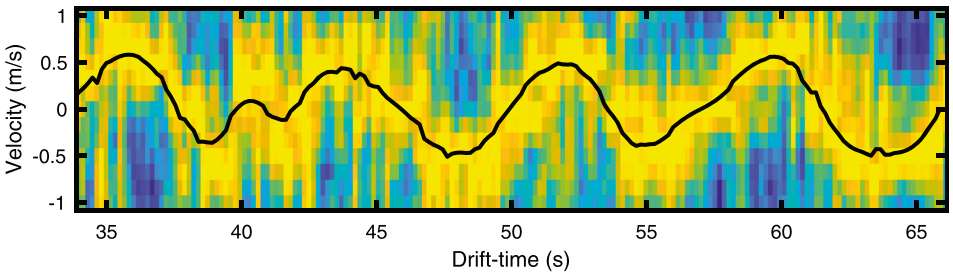

FIG. 6. (Color online) Identical to Fig. 5 with a single smoothed line superimposed.

Now the results of steps (6) and (7) still apply but S_k can be written as

$$S_k = q_k^U \times (q_k^D)^* = \sum_{j=1}^{N} x_{j,k}^U \times \exp\left(iz_j 2\pi f_k^U/c\right) \times \left(\sum_{j=1}^{N} x_{j,k}^D \times \exp\left(-iz_j 2\pi f_k^D/c\right)\right)^*, \quad (10)$$

and this can be written as $\mathbf{w_D}^\dagger \mathbf{C} \mathbf{w_U} = \mathbf{w_D}^\dagger \mathbf{H} \mathbf{w_U}$, as noted by Harrison (2017), but with a redefinition of $\mathbf{C}$ (at each frequency) as (a time-averaged)

$$\mathbf{C} = \mathbf{x_D} \times \mathbf{x_U}^\dagger, \quad (11)$$

where $\mathbf{x_D}$ and $\mathbf{x_U}$ are the results of a single (temporal) FT but interpolated, respectively, to the down- and up-shifted frequencies. At each frequency they are each vectors of length N, the number of hydrophones. The fact that this can be written as a matrix means that any operation, such as adaptive beam forming, can be modified in this way to accommodate array or target motion. It is straightforward to demonstrate the fact numerically. Also it has been found by trial and error that the most important velocity effects stem from this product [i.e., the interpolation in step (5)] rather than any modification of the steering vectors.

IV. CONCLUSIONS

A. Findings

A crude simulation of the effect of a Doppler mismatch between upward and downward paths was made using stretched and shrunk versions of a single filtered random number sequence, on the assumption that the more complicated issue of emergence of the Green's function had been investigated elsewhere and was already well understood. An example of the broadening of the cross-correlation peak was shown in Fig. 1, and the variation of peak width and peak height with velocity shown in Fig. 2. Since the cross-correlation is the integral of the product of the stretched and shrunk waveforms, it was informative to inspect their behaviour (Fig. 3). It was seen that this product rises to a maximum until, at a fairly distinct point, it levels out since the two waveforms are essentially completely unmatched from there on. A criterion for this point was given in terms of a critical time [Eq. (2)]. Given a bandwidth and a velocity, a coherent process, such as an FFT, occupying a time shorter than critical would be insensitive to Doppler shifts, whereas a longer process would benefit from the approach advocated in this paper and would be able to estimate array (or target) velocity independently of travel time.

Experimental data gathered with a drifting vertical array in the Mediterranean in 2004 were used to demonstrate that the upward and downward steered beams could be independently interpolated in Doppler-shifted frequency before forming the cross-spectrum. By repeating the analysis with a number of assumed velocities one could generate an impulse response that was a function of two-way travel time, drift-time, and velocity. Figure 4 showed that the travel time vs drift-time plot could be greatly enhanced by taking the maximum intensity over all assumed velocities. Furthermore, by finding the velocity with maximum intensity one could separate out the velocity vs drift-time as an independent measurement (Fig. 5). Having applied some smoothing, a plot of this

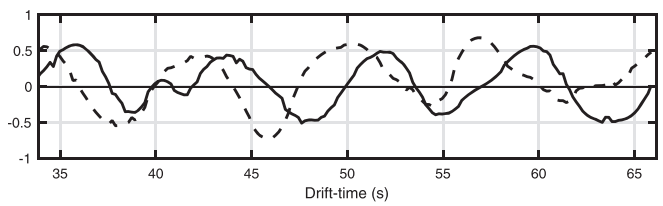

FIG. 7. The velocity smoothed line from Fig. 6 (solid line) superimposed on a single smoothed line representation of the two-way path length (dashed line) plotted against drift-time. Since the curves have different units, scaling is arbitrary.

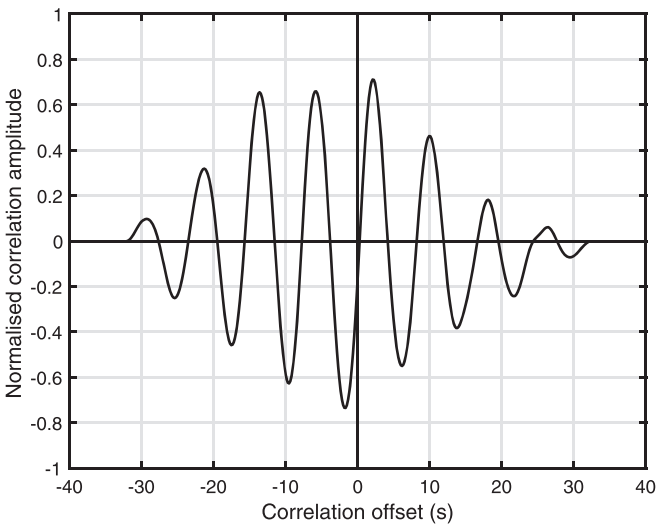

FIG. 8. Demonstration that the independently measured velocity and two-way path length from Fig. 7 are approximately 90° out of phase by cross-correlating the two quantities and observing the zero-crossing that is very close to the origin.

velocity was superimposed on the two-way path variation (Fig. 7). Finally it was demonstrated by cross-correlating velocity and travel time (Fig. 8) that the velocity was 90° phase-shifted from the travel time, as expected.

B. Implications

Up to now, PF (Harrison and Siderius, 2008) and rudimentary target detection by noise correlation (Harrison, 2008, 2016) have required the array and target to remain stationary during the necessary integration time, and this is a serious limitation in many applications. However DPF offers two new benefits: (1) longer integration times may be available; (2) an independent estimate of the velocity difference between the array and the reflector/target is available assuming no *a priori* information. This has a number of implications.

- AUVs or gliders equipped with a vertical array may continue to process while under way in a glide path, obviating the need to stop.
- Targets (glass spheres) have been detected when in line with the array (Harrison, 2008) and other plausible physical arrangements have been suggested though not verified (Harrison, 2016). The fact that motion no longer hinders processing suggests application to harbour surveillance and divers.
- This paper specifically discussed the effect of vertical motion of the receiving array with a stationary seabed. However the same reasoning and processing applies to the case where the array is fixed but the target moves radially.
- The processing described in this paper is fairly unsophisticated; instead one might consider iterative schemes. For instance, in a first pass use a small FFT to get travel time variation (as opposed to Doppler velocity) and deduce a rough velocity from its variation; in later passes with a larger FFT and Doppler processing, concentrate on velocities close to the ones deduced in the first pass.

ACKNOWLEDGMENTS

In his Emeritus capacity the author thanks CMRE for continuing to provide work facilities. He also thanks the Chief Scientist during the experiments, Peter Nielsen, and the Captain and crew of the NRV Alliance.

Crochiere, R., and Rabiner, L. R. (**1983**). *Multirate Digital Signal Processing*, in Prentice Hall Signal Processing Series (Prentice Hall, Englewood Cliffs, NJ), pp. 1–411.

Goh, S. S., and Goodman, T. N. T. (**2013**). "Estimating maxima of generalized cross ambiguity functions, and uncertainty principles," Appl. Comput. Harmon. Anal. **34**, 234–251.

Harrison, C. H. (**2005**). "Performance and limitations of spectral factorization for ambient noise sub-bottom profiling," J. Acoust. Soc. Am. **118**, 2913–2923.

Harrison, C. H. (**2008**). "Target detection and location with ambient noise," J. Acoust. Soc. Am. **123**, 1834–1837.

Harrison, C. H. (**2009**). "Anomalous signed passive fathometer impulse response when using adaptive beam forming (L)," J. Acoust. Soc. Am. **125**, 3511–3513.

Harrison, C. H. (**2016**). "Is acoustic noise and variability a nuisance or a potential tool?," Proc. Inst. Acoust. (UK) **38**(3), 168–178.

Harrison, C. H. (**2017**). "Separation of measured noise coherence matrix into Toeplitz and Hankel parts," J. Acoust. Soc. Am. **141**, 2812–2820.

Harrison, C. H. (**2018**). "The ocean noise coherence matrix and its rank," J. Acoust. Soc. Am. **143**, 1689–1703.

Harrison, C. H., and Siderius, M. (**2008**). "Bottom profiling by correlating beam-steered noise sequences," J. Acoust. Soc. Am. **123**, 1282–1296.

Muzi, L., Siderius, M., Quijano, J. E., and Dosso, S. E. (**2015**). "High-resolution bottom-loss estimation using the ambient-noise vertical coherence function," J. Acoust. Soc. Am. **137**, 481–491.

Quijano, J. E., Dosso, S. E., Dettmer, J., Zurk, L. M., Siderius, M., and Harrison, C. H. (**2012**). "Bayesian geoacoustic inversion using wind-driven ambient noise," J. Acoust. Soc. Am. **131**, 2658–2667.

Roux, P., and Kuperman, W. A. (**2004**). "Extracting coherent wave fronts from acoustic ambient noise in the ocean," J. Acoust. Soc. Am. **116**, 1995–2003.

Roux, P., Sabra, K. G., Kuperman, W. A., and Roux, A. (**2005**). "Ambient noise cross correlation in free space: Theoretical approach," J. Acoust. Soc. Am. **117**, 79–84.

Sabra, K. G., Roux, P., and Kuperman, W. A. (**2005**). "Emergence rate of the time-domain Green's function from the ambient noise cross-correlation function," J. Acoust. Soc. Am. **118**, 3524–3531.

Siderius, M., Harrison, C. H., and Porter, M. B. (**2006**). "A passive fathometer technique for imaging seabed layering using ambient noise," J. Acoust. Soc. Am. **120**, 1315–1323.

Siderius, M., Song, H., Gerstoft, P., Hodgkiss, W. S., Hursky, P., and Harrison, C. (**2010**). "Adaptive passive fathometer processing," J. Acoust. Soc. Am. **127**, 2193–2200.

Traer, J., and Gerstoft, P. (**2011**). "Coherent averaging of the passive fathometer response using short correlation time," J. Acoust. Soc. Am. **130**, 3633–3641.

Yardim, C., Gerstoft, P., Hodgkiss, W., and Traer, J. (**2014**). "Compressive geoacoustic inversion using ambient noise," J. Acoust. Soc. Am. **135**, 1245–1255.

Document Data Sheet

Security Classification		Project No.
Document Serial No.	**Date of Issue**	**Total Pages**
CMRE-PR-2019-032	May 2019	7 pp.

Author(s)

Chris H. Harrison

Title

Doppler passive fathometry

Abstract

Passive fathometry is a technique whereby broadband ambient ocean noise received on an array of hydrophones is averaged and cross-correlated to produce a sub-bottom profile [Siderius, Harrison, and Porter (2006). J. Acoust. Soc. Am. 120, 1315–1323]. Here this technique is extended to determine the vertical velocity of the array, and compensate for it, without any prior knowledge, i.e., Doppler Passive Fathometry. For Fourier transform lengths beyond a certain limit, the differing Doppler between the direct and bottom reflected paths spoils the correlation match, however it is shown by using some experimental data, where the array was known to suffer from arbitrary but near periodic motion, that compensation is possible, enabling continuing time integration. In the process, the vertical velocity becomes known. Velocity, with peak value ~±1 m/s, is plotted against time and shown to be 90° out of phase with depth, as expected for periodic motion. Since stationary targets have already been detected by noise correlation [Harrison (2008). J. Acoust. Soc. Am. 123, 1834–1837], it is implied that the range of moving targets can also be determined.

Keywords

Linear filters, underwater acoustics, geoacoustic inversion, depth profiling techniques, acoustic noise, doppler effect, geophysical instruments, optical signal processing, hydrophone, speed of sound

Issuing Organization

NATO Science and Technology Organization
Centre for Maritime Research and Experimentation

Viale San Bartolomeo 400, 19126 La Spezia, Italy

[From N. America:
STO CMRE
Unit 31318, Box 19, APO AE 09613-1318]

Tel: +39 0187 527 361
Fax:+39 0187 527 700

E-mail: library@cmre.nato.int